LS Note No. 209

July 27, 1992

Effect of Vacuum Chamber Eddy Current and Compensation by Digital Feedback

Y. Chung

Advanced Photon Source
Argonne National Laboratory
Argonne, IL 60439

Abstract

Measurement of the effect of the eddy current induced in the APS storage ring vacuum chamber by the storage ring sextupole magnet and its compensation using digital feedback with proportional, integral, and derivative (PID) control algorithm are presented. The magnetic field in the vacuum chamber shows strong quadrupole and sextupole components varying with frequency, in addition to significant attenuation and phase shift. Large changes in the magnet resistance and inductance were also observed. Development of a theory of digital feedback to obtain system responses and the conditions for optimal control will be described, in conjuction with design of a digital filter to compensate for the eddy current effect.

1. Introduction

In the APS storage ring, an extensive beam position correction system will be implemented comprising many corrector magnets (318 total) and BPMs monitoring the positions of the positron and photon beams. The AC corrector magnets, which will correct beam motion of up to 100 μrad at 25 Hz, induce eddy current in the relatively thick (1/2") aluminum vacuum chamber of the storage ring. The attenuation and phase shift of the magnet field due to this eddy current was measured and compensated for in previous works[1–3] using analog filters and a dipole magnet used for the Electron Cooling Ring Experiment at Fermilab.[4] In order to eliminate the problems characteristic of analog circuits, e.g., drift, offset, and sensitivity to temperature change, we will use in this work digital signal processing (DSP) and digital closed loop feedback to control the magnetic field in the vacuum chamber.

A prototype of the storage ring sextupole magnet was used in this work, which has geometry similar to that of the six–pole horizontal/vertical corrector magnet. The effect of the eddy current in the 0.025"–thick magnet laminations was measured and found to be negligibly small in a previous work.[5]

This note will be largely divided into two parts. The first part will describe measurement of the effect of the vacuum chamber eddy current on the horizontal and vertical magnetic fields as functions of frequency and position. Measurement of frequency dependence of the magnet impedance will also be presented. In the second part, we will develop a theory of digital closed loop feedback using analytical methods and present measurement results on the vacuum chamber eddy current effect and its compensation using digital signal processing (DSP).[6,7]

2. Measurement Setup

Figure 2.1 shows the mechanical and electrical setup for the measurements described in this note. The magnet shown in Fig. 2.1(a) is the storage ring H/V corrector magnet, which has geometry similar to that of the sextupole magnet used in this work. The magnet has main coil windings on all 6 poles and correction coil windings on the 4 side poles. Only the main coil windings were used for this work. The magnet has the effective length of 28.7 cm,[8] and the vacuum chamber was 4' (122 cm) long. A portion of the vacuum chamber was cut away from the positron beam chamber section to fit it in the magnet bore and to reduce eddy current effect.

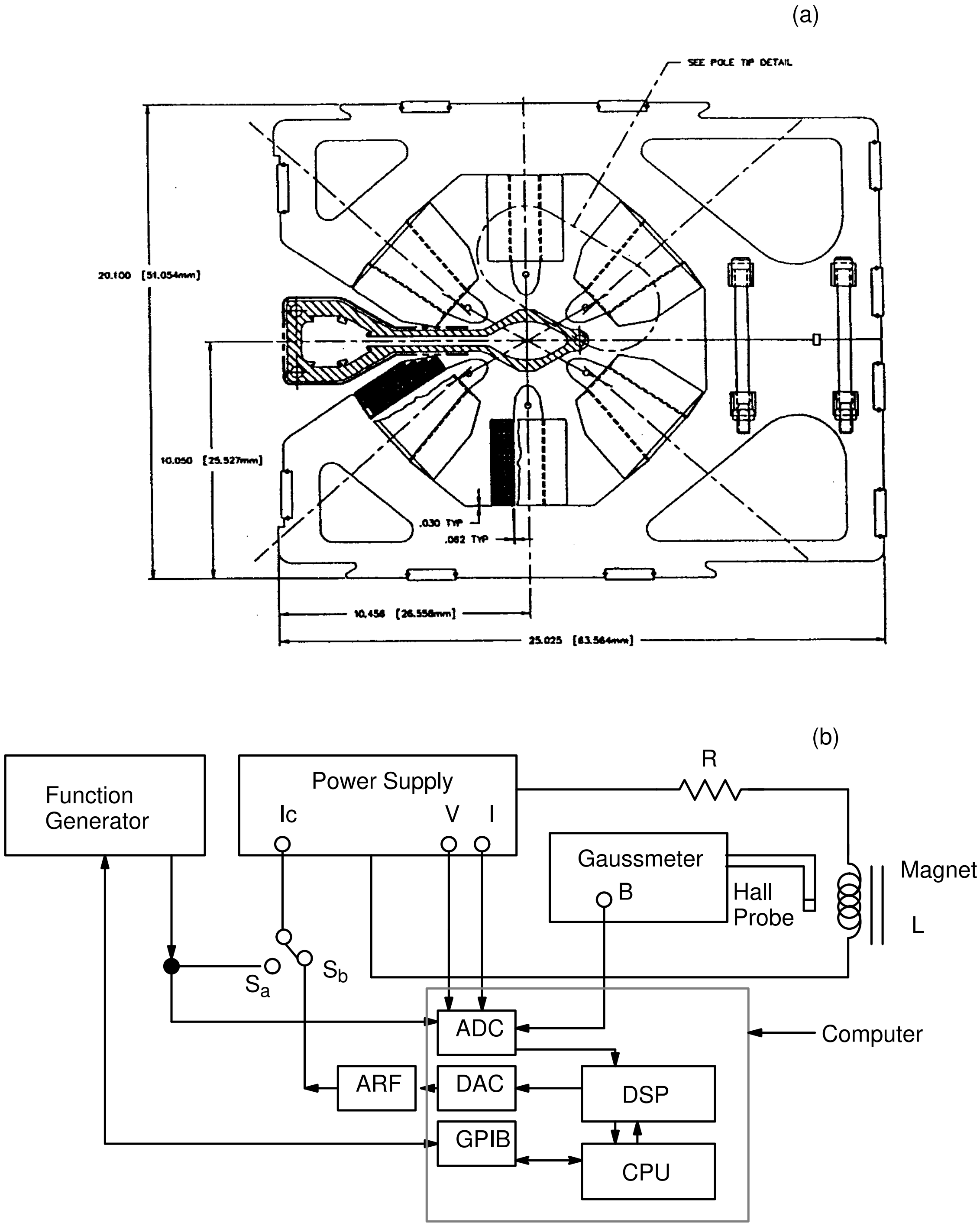

Fig. 2.1: (a) Vacuum chamber cross section in the storage ring H/V corrector magnet, similar to the sextupole magnet used in this work. (b) Schematic diagram of measurement setup for the eddy current effect on the magnet field. The voltage (V) and the current (I) signals were provided by the power supply and the magnet field (B) was measured by a gaussmeter with a Hall probe. The ADC and DAC are on the ATMIO–16 board. ARF is an analog reconstruction filter with 200 Hz bandwidth.

To simulate the control signal and the noise, e.g., ground vibration and magnet current fluctuation, a function generator (HP Model 3245A) was used. The magnet field was measured using the series 9900 menu–driven multi–channel gaussmeter manufactured by F.W. Bell. The full–scale analog output signal level is ±3V.

The power supply was a Kepco bipolar operational power supply/amplifier, model No. BOP 20–20M, with voltage range of ±20V, maximum current of 20A, and bandwidth of 10 kHz (–3 dB attenuation). The current–controlled mode was used for this work. For open loop measurements the current control signal port (I_c) was connected to the function generator output (S_A), and for closed loop measurements it was connected to the analog reconstruction filter (ARF, S_B). Analog voltage and current monitoring signals were provided through an interface card, which were digitized and analyzed by a computer. The full–scale signals are ±10V for both the voltage and the current.

The data acquisition and analysis was done by a computer with a 486 processor (CPU), equipped with an ATMIO–16 multifunction I/O board and a GPIB board to interface the function generator. Both of these were manufactured by National Instruments. The ATMIO–16 board, a multichannel ADC/DAC, has 16 input analog–to–digital converter (ADC) channels and two output digital–to–analog converter (DAC) channels. Configured for differential input, as in our setup, the maximum number of input channels is 8. The analog input signal range for the ATMIO–16 board is ±10V for all channels. With the digital resolution of 12 bits, the conversion formula is

$$\text{V (in analog)} = \frac{10}{2,048}\,\text{V (in digital)}. \tag{2.1}$$

This gives a resolution of approximately 5 mV.

Given a nominal frequency supplied by the user, the actual frequency is first found by counting the integer number of periods and the time elapsed as measured using the clock on the ATMIO board. Using this frequency f, the data is fit to the function

$$V = V_0 \cos\,(2\pi f t + \phi) \tag{2.2}$$

using linear least squares method,[9] which gives the amplitude V_0 and the phase ϕ. This procedure is done for the voltage, current, and magnet field, and the amplitudes and phases are compared to obtain the resistance and inductance of the magnet and the attenuation and phase shift of the field due to the eddy current.

The analog–to–digital conversion was done at the maximum rate of 100 ksamples/sec, which introduces a timing error of 10 µsec between two adjacent channels. With sinusoidal signal of frequency f, the phase measurement error per Hz per channel is

$$\frac{\Delta\phi\ \text{(degrees)}}{f\ \text{(Hz)}} = 3.6 \times 10^{-3}. \tag{2.3}$$

The result of measurement on $\Delta\phi/f$ at the frequencies of 10, 100, and 200 Hz is shown in Table 2.1. This phase error was compensated for in the subsequent measurements.

Table 2.1: Measurement results of the phase delay between channels 1, 2, and 3 of the ATMIO–16 board**.**

Frequency (Hz)	$\Delta\phi/f$ (degrees/Hz) between Channels 1&2	$\Delta\phi/f$ (degrees/Hz) between Channels 1&3
10	–3.50E–03 ± 1.61E–04	–7.05E–03 ± 2.38E–04
100	–3.59E–03 ± 1.59E–05	–7.19E–03 ± 1.86E–05
200	–3.60E–03 ± 4.57E–06	–7.21E–03 ± 7.15E–06

3. Measurement of Magnet Impedance

Let us write, assuming harmonic time dependence $e^{-i\omega t}$,

$$\frac{V}{I} = \left|\frac{V}{I}\right| e^{i\phi} = R - i\omega L, (3.1)$$

which gives

$$R = \frac{V}{I}\cos\phi \quad \text{and} \quad L = -\frac{1}{\omega}\frac{V}{I}\sin\phi. \tag{3.2}$$

ϕ is the phase shift between the current and the voltage. For an inductive load, such as a magnet, ϕ is negative. The current I and the field B are related by

$$B = C\ I\ a e^{-i\varphi}, \tag{3.3}$$

where C is a factor that normalizes a to 1 at DC, and a and φ are the attenuation factor and the phase shift primarily due to the vacuum chamber eddy current. To avoid the offset calibration error in the output monitoring signals provided by the power supply, an AC signal of very low frequency, say 0.1 Hz, was applied instead of a DC signal to measure the amplitude ratio. The current was maintained at ≈1 A, which produced a magnetic field of ≈12 G at DC, and the scale on the gaussmeter was set to 30 G.

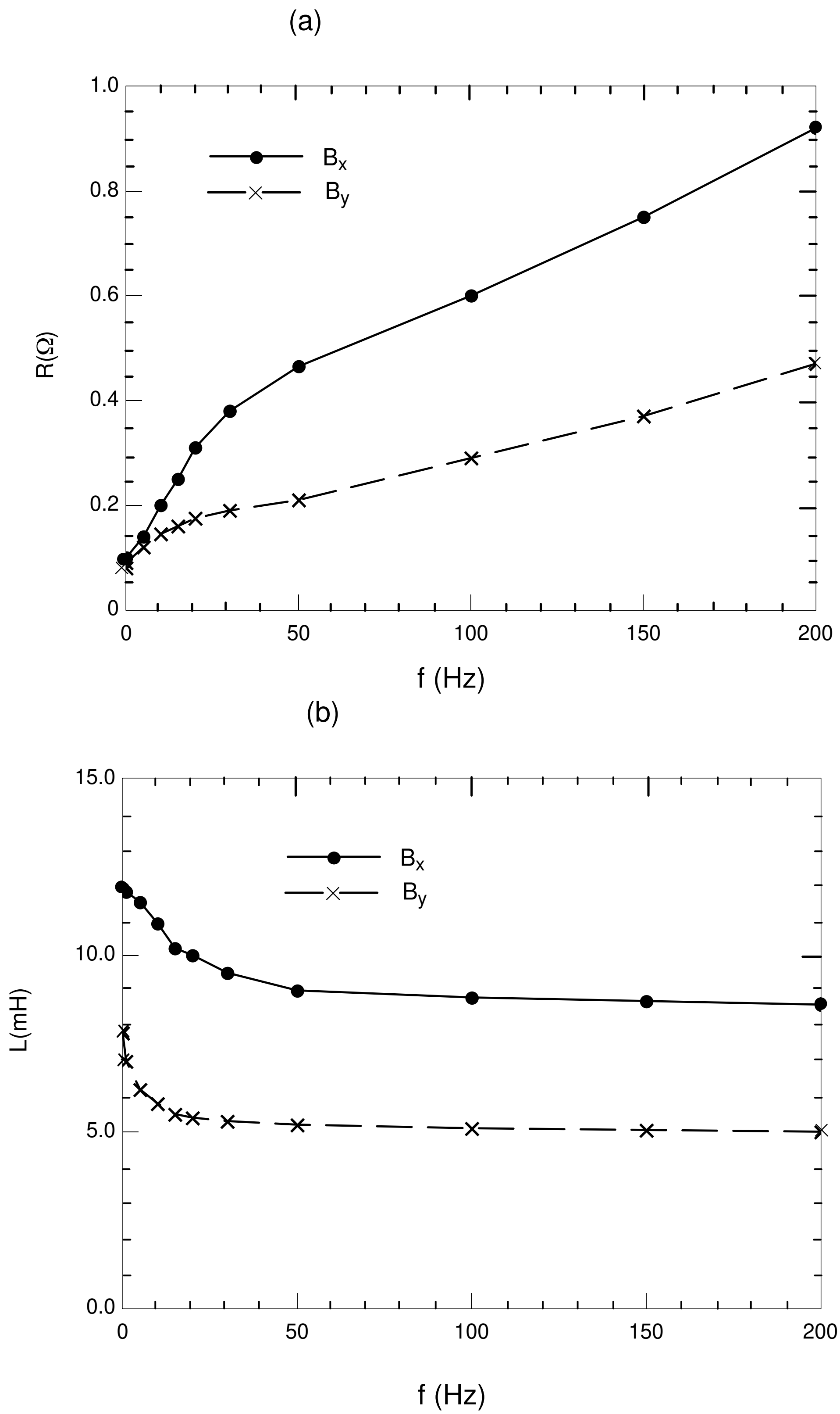

Fig. 3.1: Change of magnet impedance due to the vacuum chamber eddy current as a function of frequency: (a) resistance R in units of Ω and (b) inductance L in units of mH.

Figure 3.1(a) shows the results of measurements on the resistance of the magnet connected as vertical and horizontal correctors and Fig. 3.1(b) shows the results of measurements on the inductance. The large change in the magnet impedance with increasing frequency is mainly attributable to the eddy current in the vacuum chamber. The effect of the eddy current in 0.025”–thick magnet laminations is negligible.[5]

4. Measurement of Field Attenuation and Phase Shift

Attenuation and phase shift of the magnetic field relative to the driving magnet current were measured in a manner similar to measurement of the magnet impedance as described in the previous section, and the amplitude ratio and phase difference between the field B and the magnet current I were measured.

In Fig. 4.1(a) and 4.1(b) are shown the attenuation and phase shift of the field relative to the magnet current as functions of frequency at the center of the vacuum chamber ($x = 0$). The vertical field shows stronger attenuation and phase shift with frequency than the horizontal field, though the horizontal field appears to catch up in the high frequency region. Qualitatively, this is due to the geometry of the magnet poles and the vacuum chamber, which is vertically a little thinner but has a much larger surface cutting the magnetic flux than horizontally. This large aspect ratio and proximity of the magnet poles to the surface may create a more unfavorable condition for the vertical than the horizontal field.

Figures 4.2(a) and 4.2(b) show behavior of the magnetic field in the vacuum chamber as a function of the frequency and the horizontal distance x from the center. The antechamber side of the storage ring vacuum chamber is the positive direction. The magnetic field was measured at the positions $x = -10, -5, 0, 5$, and 10 mm relative to the center of the vacuum chamber and at various frequencies. The data measured at the frequencies $f = 0.1, 5, 20, 50, 100$, and 200 Hz are shown. Both the amplitude and phase show strong dependence on frequency and position. When the frequency is low (below 20 Hz), the quadrupole component of the magnetic field increases with frequency. Assuming harmonic time dependence $e^{-i\omega t}$, we write the vertical component of the magnetic field B_y as

$$B_y(x,\omega) = B_{y0}(\omega)\left[1 + b_1(\omega)x + b_2(\omega)x^2\right]. \quad (y = 0) \tag{4.1}$$

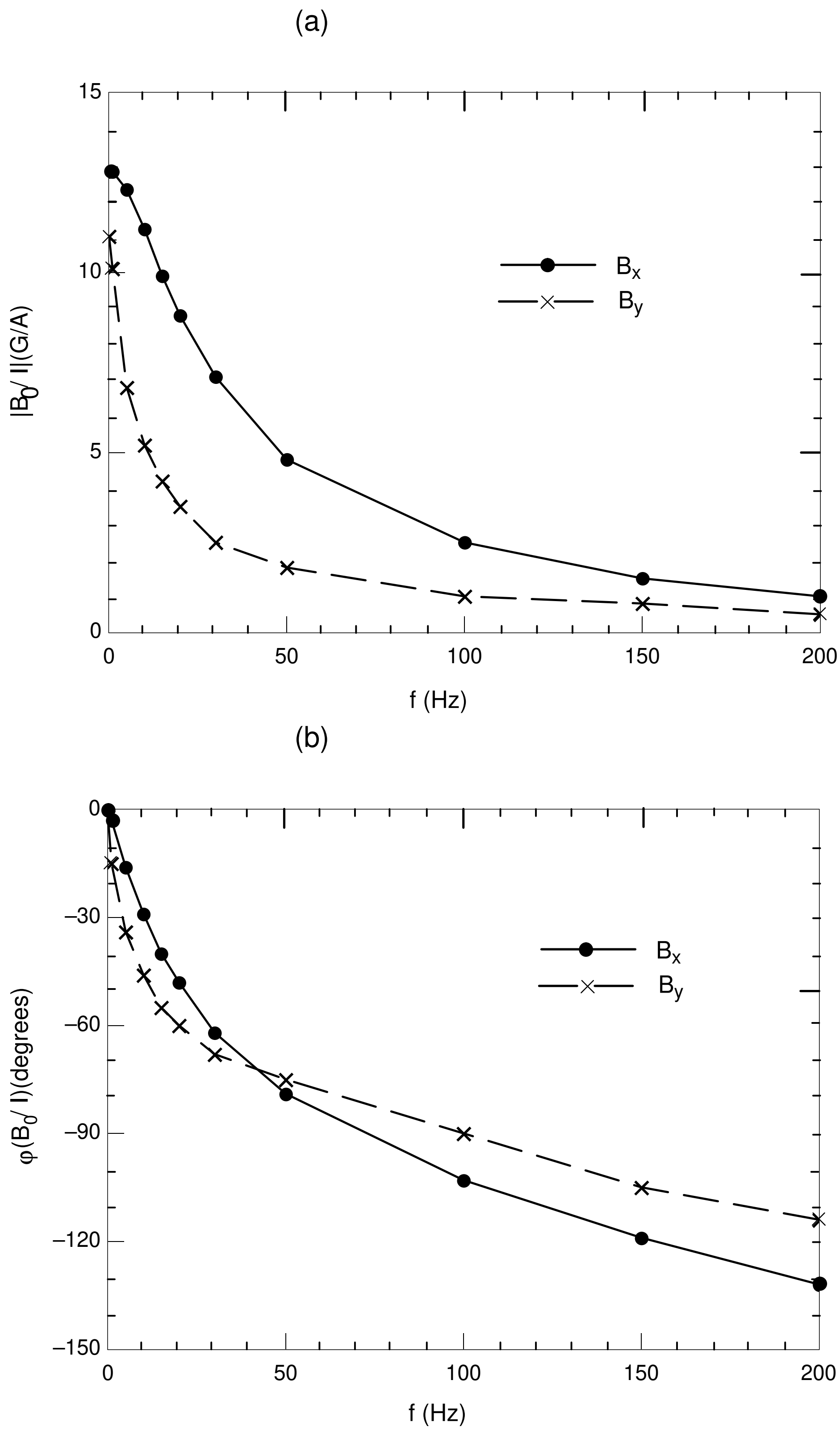

Fig. 4.1: (a) Attenuation of the field efficiency $|B_{x,y0}/I|$ and (b) phase shift φ between the field and the current as functions of frequency at the center of the vacuum chamber (x = 0).

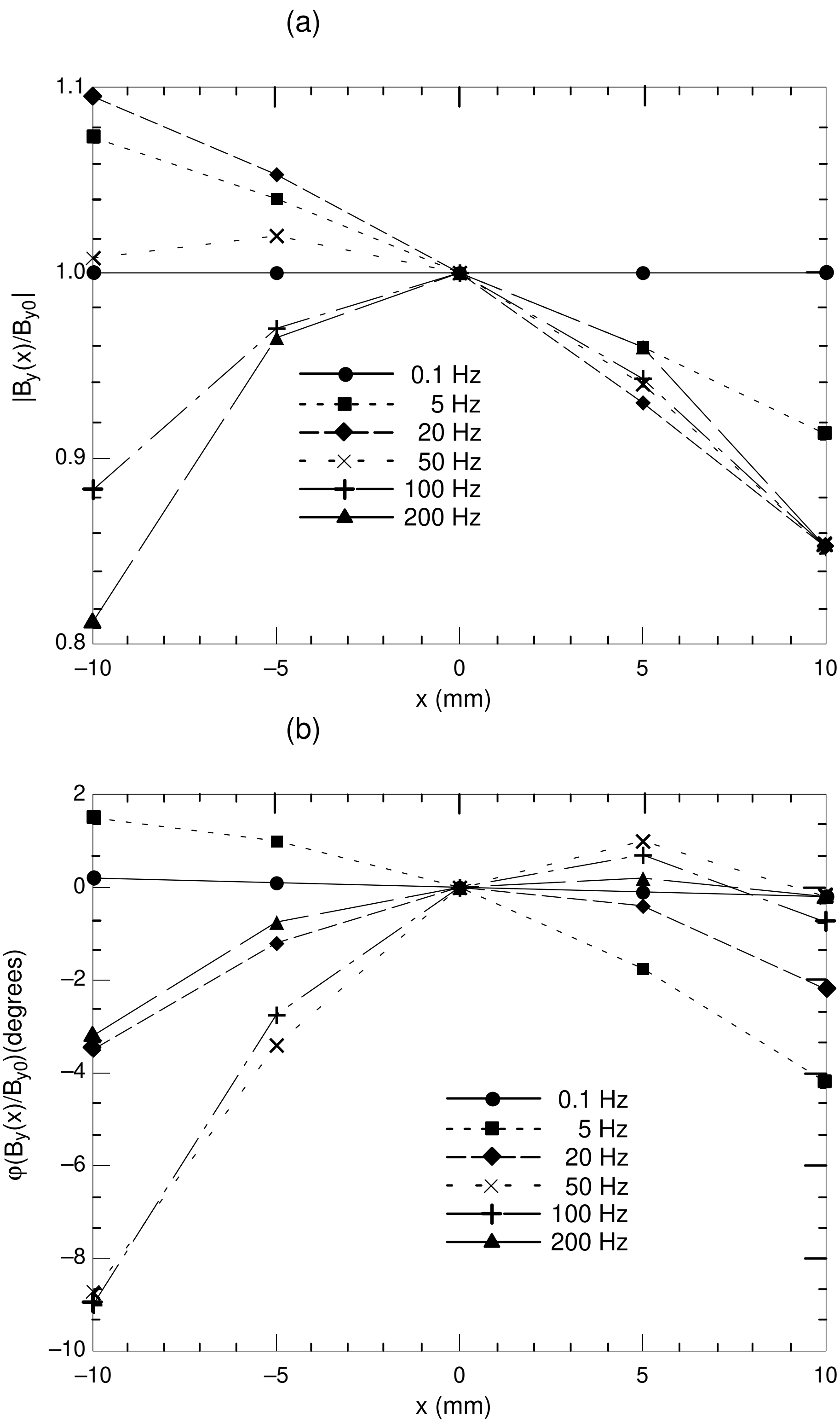

Fig. 4.2: Dependence of the magnetic field in the vacuum chamber on the position and the frequency. x is the horizontal distance from the center where the field was measured. The antechamber side is the positive direction. (a) Amplitude attenuation and (b) phase delay relative to the center (x = 0).

b_1 is the dipole coefficient and b_2 is the sextupole coefficient. The horizontal field component B_x can be expanded in a similar form. In this work, the horizontal field was measured only at the center (x = 0, y = 0) for $B_{x0}(\omega)$ at several different frequencies. The amplitude and phase of the center fields B_{y0} and B_{x0} show very strong dependence on the frequency of the driving current due to the eddy current in the vacuum chamber.

The coefficients $b_1(\omega)$ and $b_2(\omega)$ are complex numbers varying with frequency. That is, we can write

$$b_1(\omega) = b_{1r}(\omega) + ib_{1i}(\omega) \quad \text{and} \quad b_2(\omega) = b_{2r}(\omega) + ib_{2i}(\omega). \tag{4.2}$$

The values of b_{1r}, b_{1i}, b_{2r}, and b_{2i} are listed in Table 4.1 and are plotted in Fig. 4.3. Below 50 Hz, which is the frequency range of our interest for beam position correction, the quadrupole components dominate, and beyond 100 Hz, the sextupole components dominate. The strong quadrupole coefficient, which increases rapidly in magnitude in the low frequency range [0, 20] Hz, is a cause for concern. For local beam position feedback, which employs four corrector magnets to adjust the angle and displacement of the photon source, the corrector magnet field in the vacuum chamber must be very uniform to prevent local bump closure error. The good–field requirement on the corrector magnet field is[10]

$$\frac{\Delta B}{B_0} < 8 \times 10^{-3}, \quad \text{for } |x| \leq 3.2 \text{ mm}. \tag{4.3}$$

Using $b_{1r} = -0.12$ and $b_{1i} = 0.017$ at f = 20 Hz, we have

$$\frac{\Delta B}{B_0} \approx 0.039 \quad \text{at } |x| = 3.2 \text{ mm}, \ f = 20 \text{ Hz} \tag{4.4}$$

which is about 5 times larger than required by Eq. (4.3).

5. Theory of Digital Closed Loop Feedback

In this section, we will develop a theory of digital closed loop feedback using proportional (P) control. We will first start with analysis of the simplest of closed loop feedback systems with only one element, a gain of G, and show that the system is not usable. We will then insert one or more filtering elements in series with the gain in the feedback loop and analyze the system for stability. Particularly, we will derive the condition for stability and for the optimal control of a feedback system in terms of the open loop gain, the open loop bandwidth, and the sampling frequency.

Table 4.1: Multipole components of the magnetic field in the vacuum chamber.

f (Hz)	b_{1r} (cm^{-1})	b_{1i} (cm^{-1})	b_{2r} (cm^{-2})	b_{2i} (cm^{-2})
0.1	–5.06e–05	–3.62e–03	5.62e–04	–4.12e–04
1	–1.18e–02	–3.28e–02	–4.84e–04	–6.26e–03
5	–8.11e–02	–4.67e–02	–8.70e–03	–1.87e–02
10	–1.10e–01	–2.45e–02	–1.48e–02	–3.02e–02
15	–1.20e–01	–2.52e–03	–2.15e–02	–4.05e–02
20	–1.20e–01	1.69e–02	–2.90e–02	–4.94e–02
30	–1.11e–01	4.72e–02	–4.50e–02	–6.30e–02
50	–7.37e–02	7.46e–02	–7.69e–02	–7.85e–02
100	–8.71e–03	6.31e–02	–1.37e–01	–7.58e–02
150	1.63e–02	3.99e–02	–1.59e–01	–4.50e–02
200	2.03e–02	1.98e–02	–1.67e–01	–2.35e–02

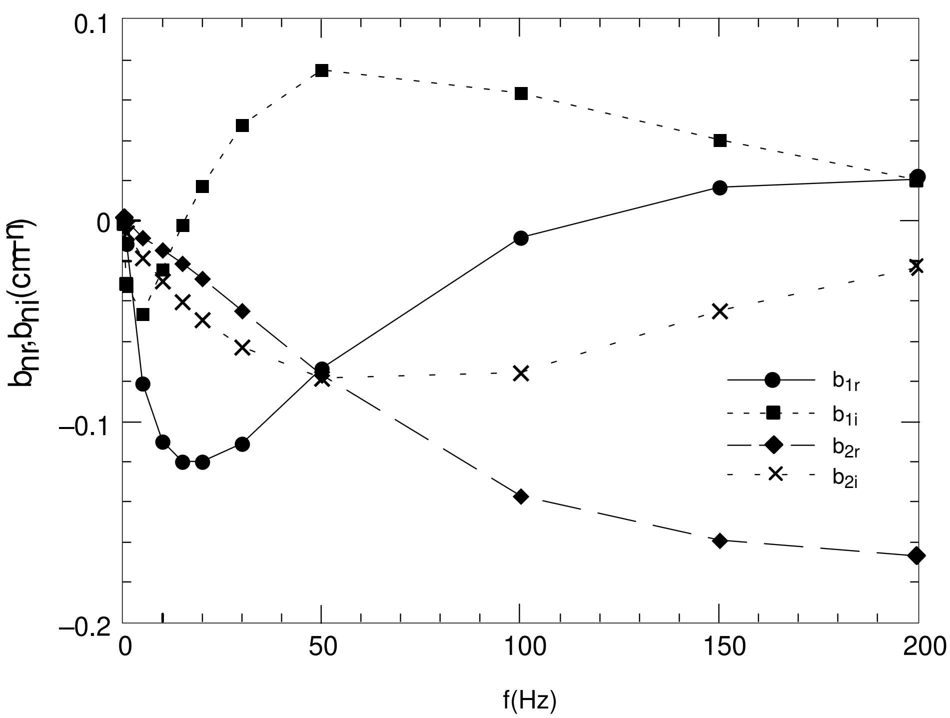

Fig. 4.3: Plotting of the multipole coefficients b_{1r}, b_{1i}, b_{2r}, and b_{2i} as functions of frequency.

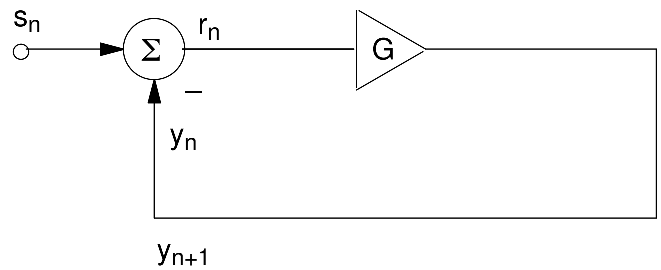

Fig. 5.1: A simple digital closed loop feedback system with open loop gain G > 0.

In Fig. 5.1 is shown a simple digital feedback system with positive open loop gain G. The discreet input sequence $\{s_n\}$ and the output sequence $\{y_n\}$ are related through

$$y_{n+1} = G(s_n - y_n). \quad (G > 0) \tag{5.1}$$

Let us for simplicity take an example of an input step impulse $\{s_n\}$ given by

$$s_n = \begin{cases} 0, & n < 0 \\ 1. & n \geq 0. \end{cases} \tag{5.2}$$

The initial condition for the output sequence $\{y_n\}$ is $y_n = 0$ for $n \leq 0$. Then the difference equation in Eq. (5.1) is solvable and the solution is given by

$$y_n = \frac{G}{1+G}(1-(-G)^n). \quad (n \geq 0) \tag{5.3}$$

We immediately see that when G is greater than 1, the feedback system is unstable. When G is less than 1, the system is stable, but the transient behavior at the onset of the step impulse is strongly oscillatory. Writing down a few terms after n = 0, we have

$$y_0 = 0, \quad y_1 = G, \quad y_2 = G(1-G), \quad y_3 = G(1-G+G^2), \tag{5.4}$$

and it finally settles to

$$\lim\, y_n = \frac{G}{1+G}. \quad (G < 1) \tag{5.5}$$

Therefore, even when G is less than one, the large overshoot and the oscillatory behavior of the system renders it unusable as a control system. Moreover, since our goal is rejection of noise perturbing the beam position, the open loop gain G needs to be larger than 1. This necessitates insertion of a low–pass filter in series with the gain in order to suppress the oscillation and stabilize the system. In the following sections, we will investigate the stability criteria of a feedback system with one or more filtering elements in the feedback loop.

5.1 Digital Feedback with One Filtering Element

To determine the relation between the sampling frequency and the bandwidth for the optimal feedback control, let us consider a simple feedback system with proportional control and a constant loop gain G as shown in Fig. 5.2.

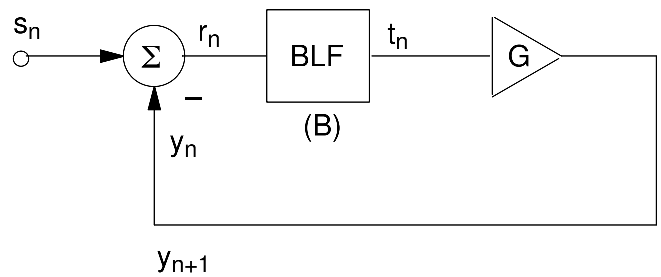

Fig. 5.2: A simple P–control closed loop feedback system.

The band–limiting filter (BLF) is a single–pole digital low–pass filter with bandwidth of f_b. The sampling frequency of the system is denoted by F_s. We will use the filter parameter c given by[5]

$$c = \cot\left(\frac{\pi f_b}{F_s}\right). \quad (5.6)$$

The signal symbols s_n, y_n, r_n, and t_n are related to each other by

$$r_n = s_n - y_n, \quad t_n = \frac{1}{1+c}\left[r_n + r_{n-1} - (1-c)\, t_{n-1}\right], \quad \text{and} \quad y_{n+1} = G\, t_n. \quad (5.7)$$

Combining the three equations in Eq. (5.7), we obtain

$$(1+c)y_{n+1} + (1-c+G)y_n + Gy_{n-1} = G(s_n + s_{n-1}). \quad (5.8)$$

This is a difference equation for the discreet sequences $\{s_n\}$ and $\{y_n\}$. The output $\{y_n\}$ should follow the given control signal $\{s_n\}$ as closely as possible without divergence. Given the initial conditions y_0 and y_1, the output of the system is uniquely defined in terms of the input.

The stability analysis of the system for general input sequence $\{s_n\}$can be done using the Z–transform.[6,7] However, to get more insight into the temporal behavior of the system, we will use Fourier analysis after rewriting Eq. (5.8) into a differential equation, assuming that the output $\{y_n\}$ is well–behaved; that is,

$$y_{n+1} - y_n << \max\ y_n. \tag{5.9}$$

Using

$$s = \frac{1}{2}(s_n + s_{n-1}),\ \ y = y_n,\ \ y' \approx \frac{1}{2}(y_{n+1} - y_{n-1}),\ \ \text{and}\ \ y'' \approx y_{n+1} - 2y_n + y_{n-1}, \tag{5.10}$$

where the prime (′) is a time derivative operator defined as

$$' \equiv \frac{1}{F_s}\frac{d}{dt}, \tag{5.11}$$

we have

$$(1 + c + G)y'' + 2(1 + c - G)y' + 4(1 + G)y = 4Gs. \tag{5.12}$$

Equation (5.12) is an inhomogeneous second–order differential equation in y. Assuming harmonic time dependence $e^{-i\omega t}$, the Fourier transform of Eq. (5.12) gives,

$$\tilde{y} = \tilde{s}\,\frac{G}{1 + G}\left(\frac{\gamma_1}{\gamma_1 - i\omega}\right)\left(\frac{\gamma_2}{\gamma_2 - i\omega}\right), \tag{5.13}$$

where eigenvalues γ_1 and γ_2 are solutions of the quadratic secular equation

$$(1 + c + G)\gamma^2 - 2(1 + c - G)\gamma F_s + 4(1 + G)F_s^2 = 0. \tag{5.14}$$

$\tilde{y}$ and $\tilde{s}$ are Fourier transforms of y and s, respectively. Equation (5.13) shows that the closed loop feedback system with a single–pole low pass filter acts like a two–pole filter. The open loop gain G and the filter parameter c determine the stability of the system through γ_1 and γ_2 as follows:

$$\begin{cases} \mathrm{Re}(\gamma_1, \gamma_2) > 0,\ \mathrm{Im}(\gamma_1, \gamma_2) = 0 & \rightarrow \text{overdamped, stable} \\ \gamma_1 = \gamma_2 > 0 & \rightarrow \text{critically damped, stable} \\ \mathrm{Re}(\gamma_1, \gamma_2) > 0,\ \mathrm{Im}(\gamma_1, \gamma_2) \neq 0 & \rightarrow \text{underdamped, stable but oscillatory} \\ \mathrm{Re}(\gamma_1) = \mathrm{Re}(\gamma_2) = 0 & \rightarrow \text{undamped} \\ \mathrm{Re}(\gamma_1) < 0 \text{ or } \mathrm{Re}(\gamma_2) < 0 & \rightarrow \text{unstable} \end{cases} \tag{5.15}$$

The feedback system is stable only when both γ_1 and γ_2 have positive real parts. From Eq. (5.14), this is satisfied if $1 + c - G > 0$. Expanding the solution of Eq. (5.14) to the first order of f_b, assuming c is large ($f_b << F_s$), we obtain

$$\frac{\gamma_1}{2\pi} \approx (1 + G) f_b \quad \text{and} \quad \frac{\gamma_2}{2\pi} \approx \frac{F_s}{\pi} - (1 + 3G) f_b. \tag{5.16}$$

These correspond to the two poles of the closed loop feedback system. We see that the closed loop bandwidth is roughly (1 + G) times the open loop bandwidth f_b.

Let us take an example of f_b = 30 Hz, F_s = 4 kHz, and G = 3. Then from Eqs. (5.6) and (5.14), the solutions are

$$c = 42.4, \quad \gamma_1 = 0.228\ F_s, \quad \text{and} \quad \gamma_2 = 1.514\ F_s, \tag{5.17}$$

and the eigenfrequencies are

$$f_1 = \frac{\gamma_1}{2\pi} = 145\ \text{Hz} \quad \text{and} \quad f_2 = \frac{\gamma_2}{2\pi} = 964\ \text{Hz}. \tag{5.18}$$

Both f_1 and f_2 are positive real, and therefore, the system is stable. The bandwidth has also been broadened by a factor of 5 from the open loop bandwidth of 30 Hz.

5.2 Digital Feedback with Multiple Filtering Elements

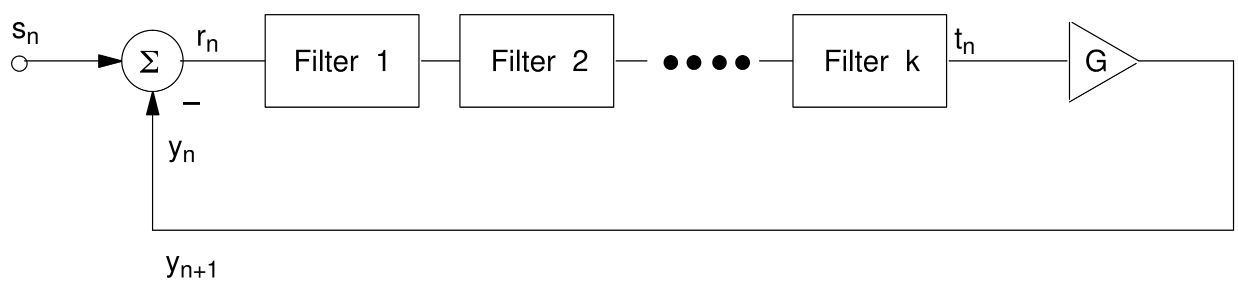

Fig. 5.3: Closed loop feedback with multiple filtering elements.

The analysis presented in the last section for a closed loop feedback system with one filtering element can be generalized to systems with multiple filtering elements connected in series as shown in Fig. 5.3. Including more filters in the system can degrade the overall performance of the system by introducing a large open loop phase shift. However, it is sometimes necessary to do so in order to prevent overshoot and oscillation when the open loop bandwidth is too large for a given sampling frequency and loop gain. For example, the beam position feedback system uses corrector magnets and beam position monitors (BPMs). When the bandwidth of the BPM is too large, it must be compensated by another low pass filter in the digital signal processing unit. Reducing the bandwidth of the BPM itself by integrating data for a longer time is not as good a solution for several reasons: 1) the number of turns required may be too large, 2) simple integration may result in oscillation due to undesirable large phase shift beyond the bandwidth, and 3) the DSP does 32–bit floating point operation and therefore is more accurate than the BPM processing unit.

The relation for the loop gain, the open loop bandwidth, and the sampling frequency of an optimally controlled closed loop feedback system will be derived in Section 5.4. In this section, we will replace analog components, such as the vacuum chamber, the magnet, and the analog reconstruction filter, with corresponding digital filters with first–order poles, so that the system response may be put in the form of Eq. (5.13).

Let us take the case of three (n = 3) filters with filter coefficients c_1, c_2, and c_3, which are given by

$$c_i = \cot\left(\frac{\pi f_i}{F_s}\right). \quad (i = 1, 2, 3) \tag{5.19}$$

f_i is the frequency of 3 dB attenuation of the i–th filter. It can be shown that the output y in the continuous domain satisfies the differential equation given by

$$d_4 y'''' + d_3 y''' + d_2 y'' + d_1 y' + d_0 y = d_0 \frac{G}{1 + G} s, \tag{5.20}$$

where

$$\begin{aligned}
d_4 &= (1 + c_1)(1 + c_2)(1 + c_3) + G, \\
d_3 &= 2((1 + c_1)(1 + c_2)(1 + c_3) - G), \\
d_2 &= 4(2 + c_1 + c_2 + c_3 + c_1 c_2 + c_2 c_3 + c_3 c_1 + 2G), \\
d_1 &= 8(1 + c_1 + c_2 + c_3 - G), \\
d_0 &= 16(1 + G).
\end{aligned} \tag{5.21}$$

The secular equation for Eq. (5.20) is

$$d_4 \gamma^4 - d_3 \gamma^3 F_s + d_2 \gamma^2 F_s^2 - d_1 \gamma F_s^3 + d_0 F_s^4 = 0. \tag{5.22}$$

With solutions γ_1, γ_2, γ_3 and γ_4 from Eq. (5.22), we have an expression similar to Eq. (5.13),

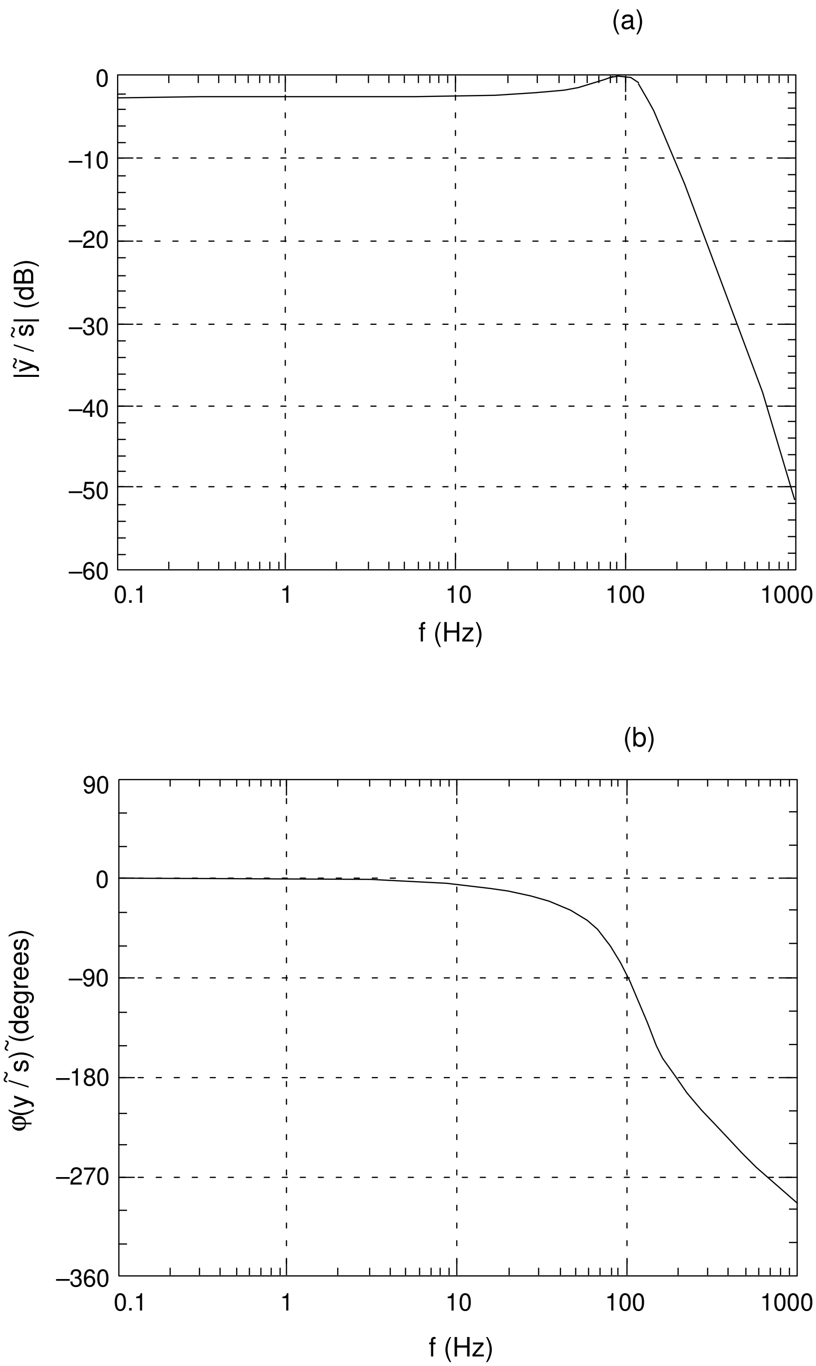

Fig. 5.4: Frequency response of the closed loop feedback system with parameters in Eq. (5.25), (a) magnitude and (b) phase. Note that there is a resonance at f ≈ 100 Hz.

$$\tilde{y} = \tilde{s}\,\frac{G}{1+G}\left(\frac{\gamma_1}{\gamma_1-i\omega}\right)\left(\frac{\gamma_2}{\gamma_2-i\omega}\right)\left(\frac{\gamma_3}{\gamma_3-i\omega}\right)\left(\frac{\gamma_4}{_4-i\omega}\right). \tag{5.23}$$

In Eq. (5.23), the overall system response resembles that of a filter with poles at $\omega = \gamma_j$ (j = 1, 2, 3, 4). This result can be generalized to the case of k poles. A feedback system with k open loop poles, counting m–th order poles as m poles, can be represented as a filter of k+1 poles in the complex plane. That is,

$$\text{k open loop poles} \rightarrow \tilde{y} = \tilde{s}\,\frac{G}{1+G}\prod_{j=1}^{k+1}\left(\frac{\gamma_j}{\gamma_j-i\omega}\right), \tag{5.24}$$

where γ_j's are solutions of the corresponding (n+1)–th order polynomial obtained by performing transformations similar to Eq. (5.10).

Let us take an example of a 3–pole system with the following parameters:

$$f_1 = 30\ \text{Hz},\quad f_2 = 100\ \text{Hz},\quad f_3 = 200\ \text{Hz},\quad \text{and}\quad G = 3. \tag{5.25}$$

From Eqs. (5.21) and (5.22), we have, in units of Hz,

$$\frac{\gamma_1}{2\pi} = 48 + 109i,\quad \frac{\gamma_2}{2\pi} = 48–109i,\quad \frac{\gamma_3}{2\pi} = 426,\quad \text{and}\quad \frac{\gamma_4}{2\pi} = 749. \tag{5.26}$$

The real parts are all positive, and, therefore, the system is stable. The imaginary parts indicate frequency shift of the system response and resonances will appear in the system response near those frequencies. This is typical of closed loop feedback and can be readily recognized using Nyquist diagrams. Figure 5.4 shows the frequency response of the system with the parameters in Eq. (5.25).

5.3 Determination of Sampling Frequency, Bandwidth, and Gain

In the last two sections we analyzed digital feedback systems with one or multiple filtering elements in the closed loop. In this section we will use the results of Section 5.1 for systems with one filter to obtain the optimal parameters for the sampling frequency, bandwidth, and gain. We will use only one filter to make the system simpler to analyze and the eigenfrequencies easier to identify. The results will later be applied to measurements on and compensation for effect of the vacuum chamber eddy current for control of the corrector magnet field in the vacuum chamber.

When the roots of Eq. (5.14) are the same ($\gamma_1 = \gamma_2$), the system is critically damped and provides the optimal control with the shortest settling time without overshoot. The open loop gain G_c that corresponds to critical damping is, from Eq. (5.14),

$$G_c = \frac{2}{3}\sqrt{3c^2 + 6c + 4} - c - \frac{5}{3} \approx 0.155c - 0.5. \qquad (5.27)$$

In the last step of Eq. (5.27), the expression in the square root was expanded assuming that c is much larger than 1. This assumption is verified immediately. The gain G_c must be large for effective control, and therefore, c must also be large. Equation (5.27) is the necessary condition for the output to be critically damped at application of a step impulse input. When G is larger than G_c, the output will be underdamped, causing oscillation. In the opposite case when G is smaller than G_c, the output will be overdamped, resulting in longer settling time. From Eqs. (5.6) and (5.27), we have, when $f_b << F_s$ and $G >> 1$,

$$\frac{F_s}{G\ f_b} \approx 20. \qquad (5.28)$$

Equation (5.28) is the basic relation for loop gain, open loop bandwidth, and sampling frequency of an optimally controlled feedback system with one bandlimiting filter connected in series with a constant open loop gain G.

In the case of a more complex PID (proportional, integral, and derivative) control, we must also consider the effect of the integral and derivative control gains, K_I and K_D. However, when K_I is small (<< 1), the frequency range of concern for loop stability is primarily covered by the proportional control action, and therefore, Eq. (5.28) with G replaced by K_P remains valid.

6. Measurement of the Vacuum Chamber Eddy Current Effect

In this section, we will present the results of measurement of the effect of the vacuum chamber eddy current on the magnet field. The setup is the same as that shown in Fig. 2.1(b) in the open loop configuration (switch S_A closed). The power supply was in the current–controlled mode, which has an internal closed loop of its own.

Figure 6.1 shows the schematic diagram for closed loop feedback with PID control for the magnetic field. There are two types of input: s_n for set points and w_n for external perturbation. In this measurement, only one of them was used at a time. When the s_n input is used, w_n is set to 0, and vice versa. In this configuration, the spectral ratio of y_n and s_n gives the system transfer function of the closed loop feedback system and the spectral ratio of y_n and w_n gives its noise transfer function.

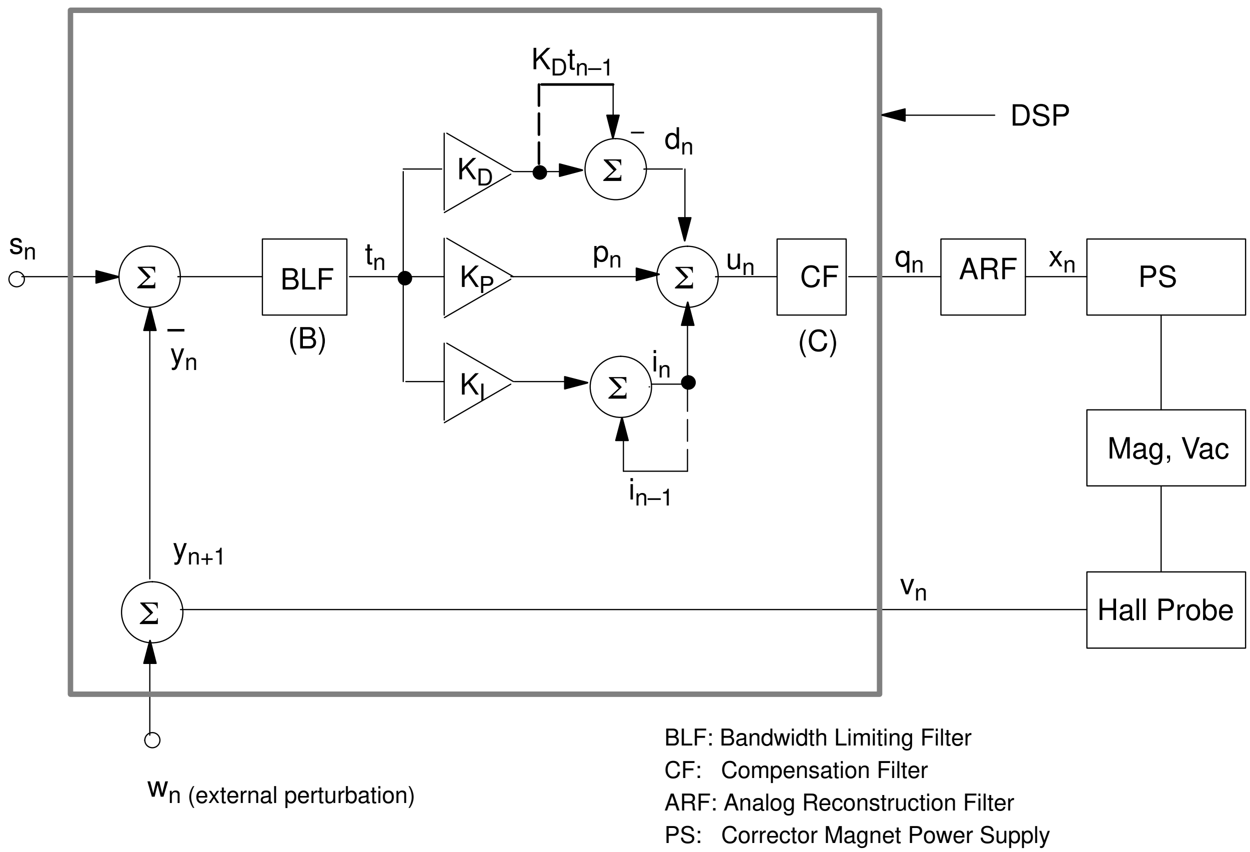

Fig. 6.1: Schematic diagram for the closed loop feedback with PID control.

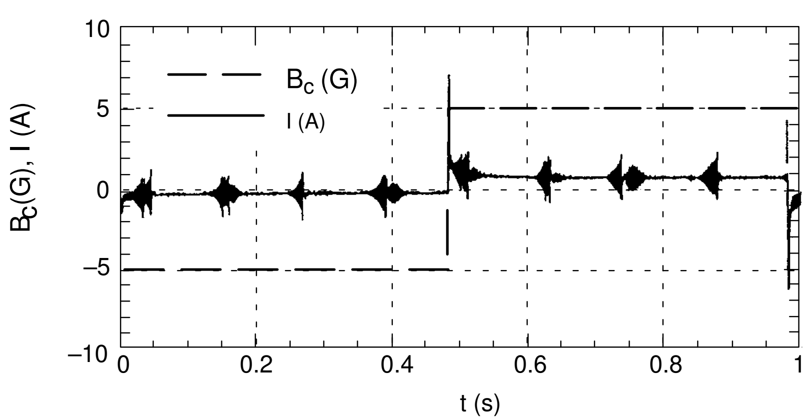

Fig. 6.2: Ringing in the magnet current with the feedback loop closed (solid line). The dotted line is the field control signal of 1 Hz square pulse. The ARF was turned off and the parameters used were: F_s = 2 kHz, f_b = 20 Hz, K_P = 3, K_I = 0.1, and K_D = 1.

The analog reconstruction filter (ARF) is an analog low pass filter of 200 Hz bandwidth. It was inserted in front of the power supply control input in order to suppress the anomalous high frequency ringing in the magnet current, as shown in Fig. 6.2, when the feedback loop was closed. It was also intended to simulate the BPM, which will have finite bandwidth due to averaging over many turns. This ringing was observed when the DSP could not keep up with the sampling frequency and failed to operate synchronously with the ADC. It was not observed when the loop was open. The backlog in the DSP causes bursts of oscillation as is observed if the open loop bandwidth is not narrow enough to suppress them.

6.1 Measurement Results and Design of Digital Compensation Filter

Figure 6.3 shows the results of measurement on the amplitude ratios and relative phases of the current control signal I_c, the actual current on the magnet I, and the magnetic field B in the vacuum chamber measured with a Hall probe in the frequency range of 0.1 Hz — 1 kHz. This apparently wide range of frequency of measurement is necessary for the design of the digital compensation filter for the eddy current.

The effect of the eddy current in the vacuum chamber is shown in the rapid decrease of the field current ratio (B/I) with frequency. The phase delay of 35° between the current control signal I_c and the magnet current I at 1 kHz is due to the internal closed loop feedback for current control. The bandwidth of the power supply in the current–controlled mode is rated at 10 kHz for –3 dB attenuation.

The attenuation and phase shift of the field B with respect to the current I has an adverse effect on the closed loop feedback by decreasing the magnet field efficiency and deteriorating the stability of the feedback loop. This can be partly remedied by inserting a digital compensation filter (CF in Fig. 6.1) in front of the power supply control input. The digital compensation filter is designed such that its input and the digitized signal from the gaussmeter have ratio close to unity within the frequency range of our interest. The measurement results of the field attenuation is normalized to dimensionless units and fitted to an expression as given by[6,7]

$$H(z) = C \prod_{k=1}^{K} \frac{1 + f_k z^{-1} + g_k z^{-2}}{1 + c_k z^{-1} + d_k z^{-2}}. \qquad (6.1)$$

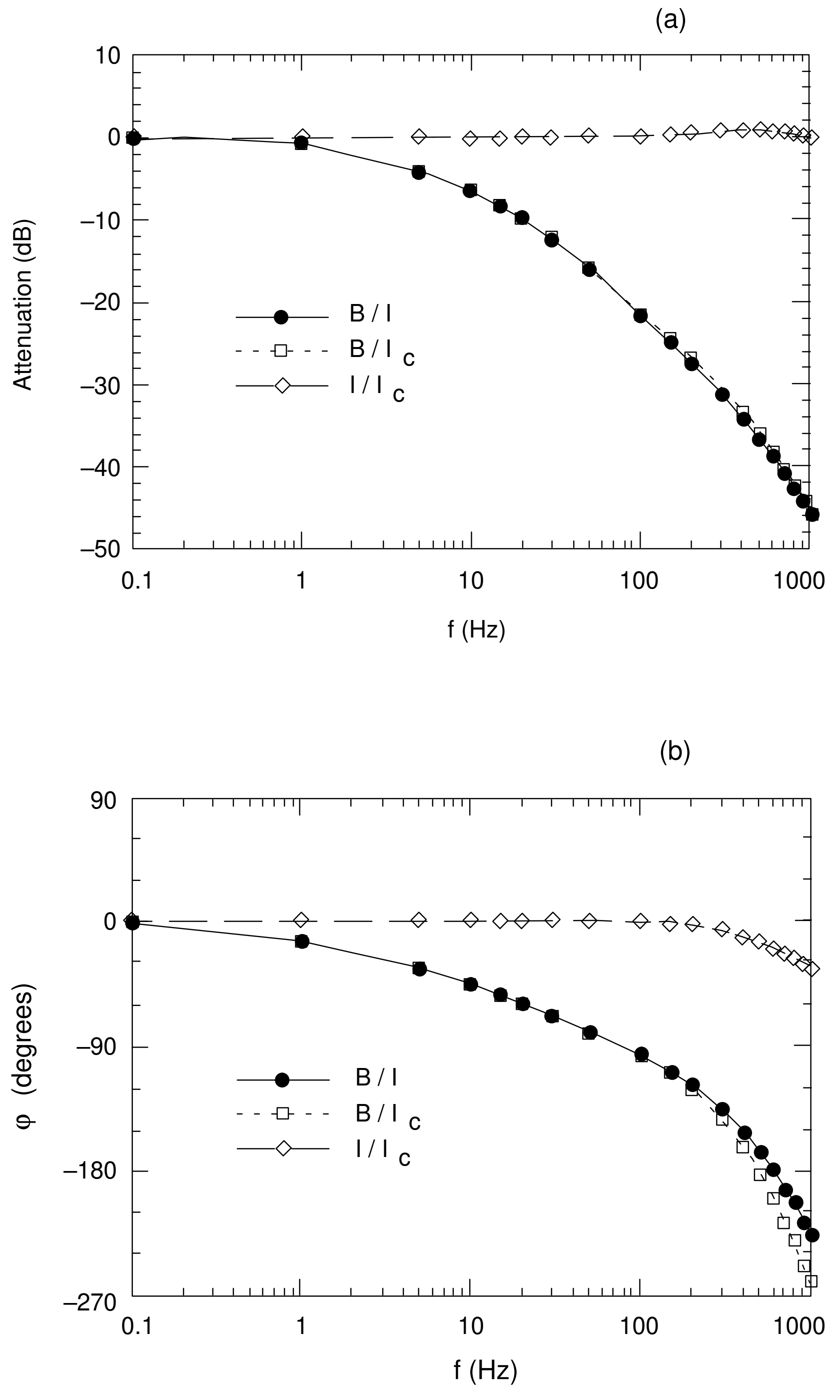

Fig. 6.3: Results of the open loop measurements on (a) the amplitude ratios and (b) the relative phases of current control signal I_c, magnet current I, and the magnetic field B in the vacuum chamber.

Here, $z = e^{-i\lambda}$ and λ is the digital frequency given by

$$\lambda = 2\tan^{-1}\left(\frac{\pi f}{F_s}\right) \approx p\,\frac{2f}{F_s} \text{ when } f << F_s. \tag{6.2}$$

The transfer function H(z) relates the Z–transforms V(z) and X(z) of the sequences $\{x_n\}$ and $\{v_n\}$ shown in Fig. 6.1 through

$$V(z) = H(z)\,X(z). \tag{6.3}$$

For more discussion on the Z–transform of discreet sequences, readers are referred to Refs. 6 and 7. The transfer function corresponding to the CF is just the inverse of H(z). Let U(z) and Q(z) be the Z–transforms of the sequences $\{u_n\}$ and $\{q_n\}$, then we have

$$Q(z) = \frac{1}{H(z)}\,U(z). \tag{6.4}$$

Putting

$$H(z) = \frac{\sum_{k=0}^{M} a_k z^{-k}}{1 + \sum_{k=1}^{L} b_k z^{-k}}, \tag{6.5}$$

we can write the inverse of H(z) as

$$\frac{1}{H(z)} = \frac{1}{a_0}\,\frac{\sum_{k=0}^{L} b_k z^{-k}}{1 + \sum_{k=1}^{M} \frac{a_k}{a_0} z^{-k}} \quad (b_0 = 1), \tag{6.6}$$

and we have

$$q_n = \frac{1}{a_0}\left[u_n + \sum_{k=1}^{L} b_k u_{n-k} - \sum_{k=1}^{M} a_k q_{n-k}\right]. \tag{6.7}$$

Using the measurement results shown in Fig. 6.3(a) and with K = 2 and F_s = 4 kHz, the best fit gives

$$C = 0.0173025$$

$$c_1 = 1.94223,\ d_1 = 0.94284,\ f_1 = -0.90665,\ g_1 = -0.08920, \tag{6.8}$$

$$c_2 = -1.21537,\ d_2 = 0.21730,\ f_2 = -0.69730,\ g_2 = -0.26649.$$

The Hall probe sensitivity of 10 G/V and the power supply control sensitivity of 2 A/V were used. From Eqs. (6.1), (6.5), (6.7) and (6.8), we obtain

$$q_n = 57.8\ (u_n - 3.1576\ u_{n-1} + 3.5207\ u_{n-2} - 1.5679\ u_{n-3} + 0.2049\ u_{n-4}) +$$

$$1.6040\ q_{n-1} - 0.2765\ q_{n-2} - 0.3038\ q_{n-3} - 0.0238\ q_{n-4}. \tag{6.9}$$

The sequence $\{u_n\}$ is in units of dimensionless computer counts converted from voltage. From Eq. (6.9), the next output of the compensation filter is calculated using the current input, 4 previous inputs, and 4 previous outputs. Since no future samples from either the input or output are needed to calculate the current output, the filter is physically realizable or causal.

6.2 Performance of the Closed Loop Feedback

Figures 6.4(a) and 6.4(b) show the results of measurements on the closed loop feedback for the corrector magnet field in the vacuum chamber. A bandlimiting filter (BLF) of 30 Hz was used for these measurements. The eddy current compensation filter was turned on and off during measurements for comparison. For the open loop measurements, B_c is the control signal at either the input of the CF (u_n, with CF) or the input of the PS (q_n, without CF) in Fig. 6.1. The ARF of 200 Hz bandwidth in front of the power supply was turned off. For the closed loop measurements, B_c is the control signal at the input of the DSP (s_n) in Fig. 6.1. The CF was turned on (with CF) or off (without CF) and the ARF in front of the power supply was turned on. These results primarily compare the system performance with and without the CF.

Compensation for the eddy current effect by the CF is almost perfect in restoring the amplitude. Still, there is significant phase delay remaining (–79° at 200 Hz), because the transfer function H(z) in Eq. (6.1) does not simultaneously model the eddy current effect perfectly in both amplitude and phase. The coefficients in Eq. (6.8) were obtained in such a manner that only the amplitude data fit $|H(z)|$ as closely as possible with K = 2.

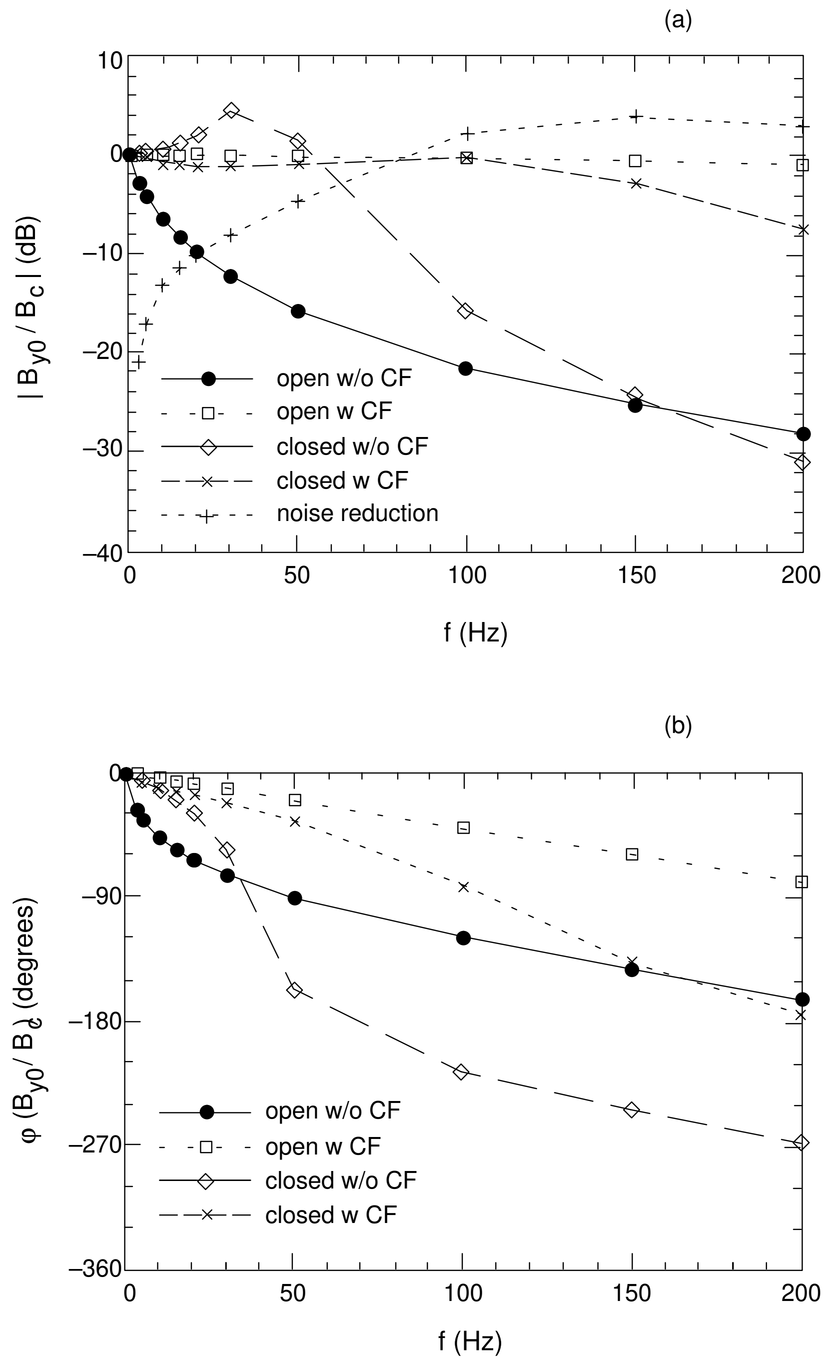

Fig. 6.4: Results of measurement on the closed loop feedback for corrector magnet field: (a) amplitude attenuation and (b) phase shift. For closed loop measurements, an analog reconstruction filter of 200 Hz bandwidth was inserted in front of the power supply to suppress ringing. The parameters used were: F_s = 4 kHz, f_b = 30 Hz, K_P = 3, K_I = 0.05, and K_D = 0.5.

Figure 6.5 shows time domain measurements of the magnetic field B inside the vacuum chamber and the magnet current I in response to the input square pulses of 15 Hz with the CF turned off. Figure 6.6 shows similar measurements with the CF turned on for comparison. The results demonstrate the clear advantage of canceling the effect of the eddy current. Without the CF, as shown in Fig. 6.5(b), the magnetic field exhibits strong oscillation. This can be explained from the analysis of Section 5.2, considering the vacuum chamber as a low–pass filter to the AC magnetic field with several poles on the imaginary axis of the complex frequency space. Closing the feedback loop adds one more pole to these and rearranges them. If some of these rearranged poles have real parts, especially those with the smallest imaginary parts, then the overall system response could amplify the low frequency components and oscillation results. This is also shown in Fig. 6.4(a), where the amplitude ratio $|B_{y0}/B_c|$ measured on the feedback loop without the CF is larger than unity below 50 Hz, with a peak at around 30 Hz, and decreases sharply. In comparison, the feedback loop with the CF shows a much cleaner response.

From this consideration, one might say that the feedback system response without the CF could be improved by broadening the bandwidth of the BLF, since locating the pole farther away from the origin will move the peak to a higher frequency. This is not necessarily true. Consider the single–pole low–pass filter transfer function

$$F(\omega) = \frac{\gamma}{\gamma - i\omega} = \frac{\gamma_r + i\gamma_i}{\gamma_r + i(\gamma_i - \omega)}. \tag{6.10}$$

At resonance ($\omega = \gamma_i$), we have

$$|F(\omega)| = \sqrt{1 + Q^2}. \qquad \left(Q = \left|\frac{\gamma_i}{\gamma_r}\right|\right) \tag{6.11}$$

Equation (6.11) shows that $|F(\omega)|$ will actually get larger, and therefore worse, if the Q–factor increases.

7. Summary

In this work, the magnet impedance and the attenuation and phase shift of the magnet field with respect to the magnet current due to the vacuum chamber eddy current were measured as functions of frequency in the range DC to 200 Hz. The magnet was the storage ring sextupole magnet with vertical correction winding, and a 4 foot–long piece of the APS storage ring vacuum chamber was inserted in the magnet bore.

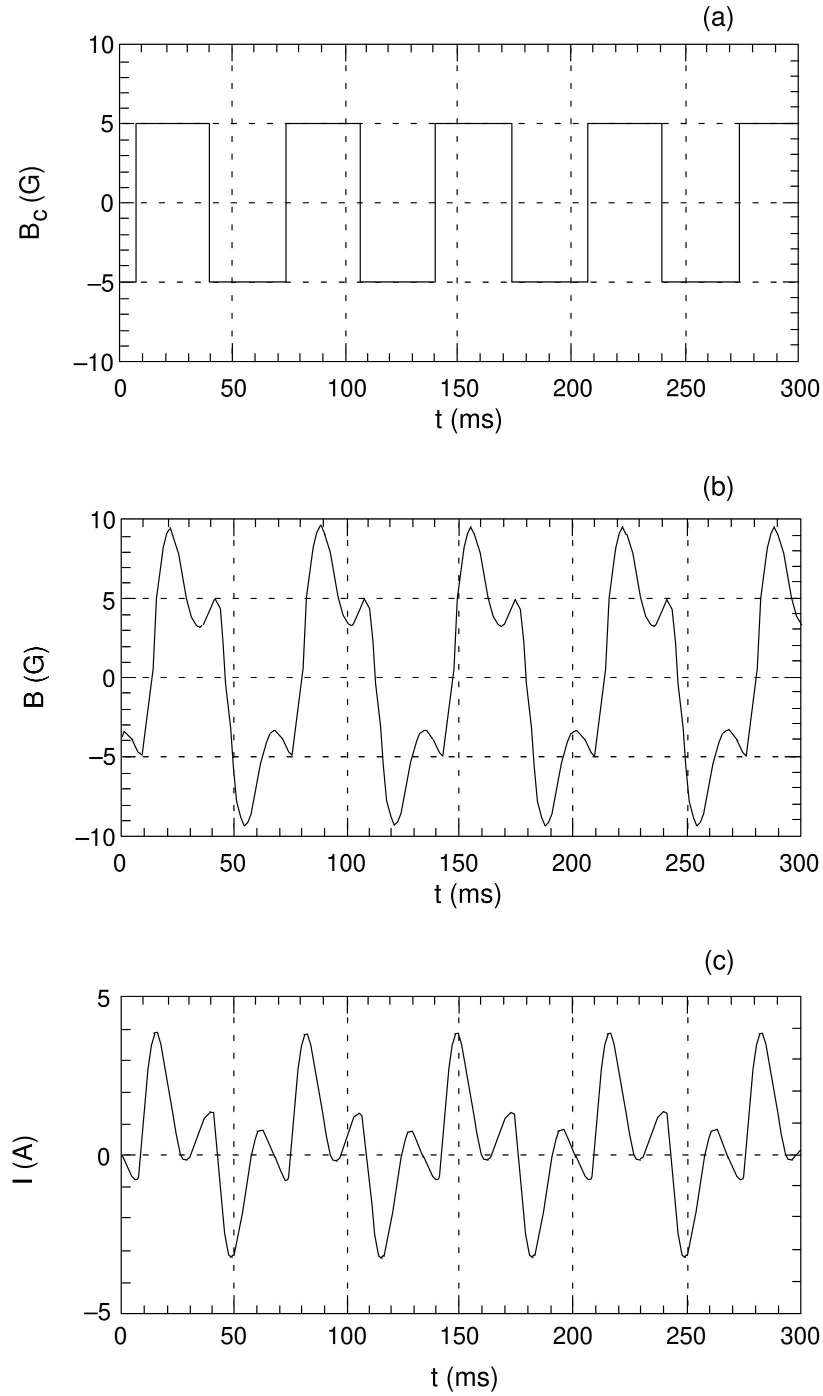

Fig. 6.5: Feedback system response in the time domain without eddy current compensation: (a) magnetic field control signal B_c (s_n, 15 Hz square wave), (b) magnetic field in the vacuum chamber (y_n), and (c) magnet current I. The parameters used were: F_s = 4 kHz, f_b = 30 Hz, K_P = 3, K_I = 0.05, and K_D = 0.5.

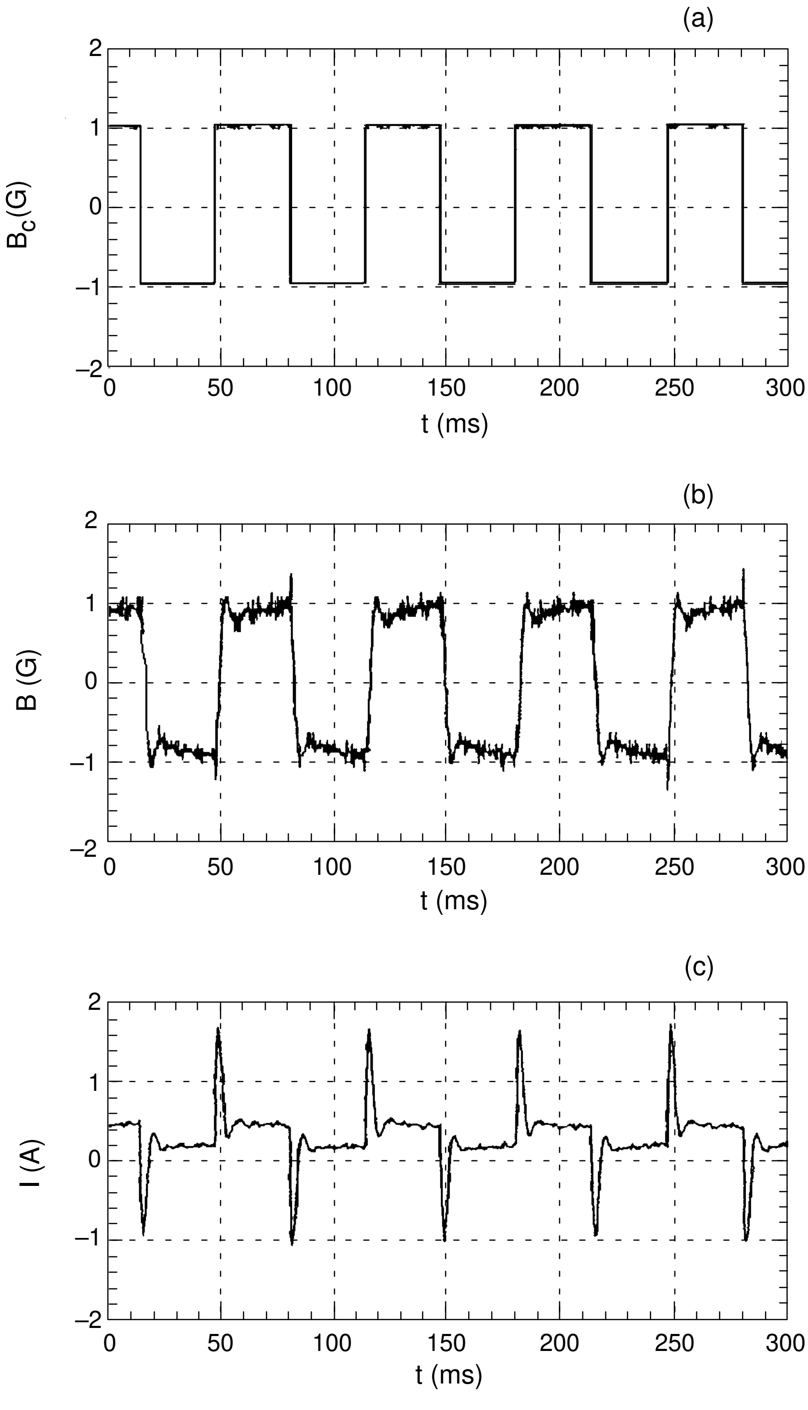

Fig. 6.6: Feedback system response in the time domain with eddy current compensation: (a) magnetic field control signal B_c (s_n, 15 Hz square wave), (b) magnetic field in the vacuum chamber (y_n), and (c) magnet current I. The parameters used were: F_s = 4 kHz, f_b = 30 Hz, K_P = 3, K_I = 0.05, and K_D = 0.5.

The results show significant attenuation and phase shift of the magnet field (–3.2 dB and –49° for B_x, and –10.1 dB and –60° for B_y at 20 Hz) in the vacuum chamber. Large changes in magnet resistance and inductance were also observed. Spatially resolved measurements of B_y at the midplane revealed strong quadrupole and sextupole components in the low frequency range below 50 Hz, which could potentially degrade global beam stability due to local bump closure error. This problem has yet to be identified in a manner rigorous and quantitative enough to be properly resolved.

Conditions for optimal control were obtained through development of a theory of digital feedback. The results were successfully applied to closed loop control of the magnetic field in the vacuum chamber in combination with the eddy current compensation filter, using digital signal processing (DSP) and a proportional, integral, and derivative (PID) control algorithm. These two, together with the singular value decomposition (SVD) technique for matrix inversion,[6,11] will be the basis for the global and local beam position feedback in the APS storage ring.

Acknowledgement

The author would like to thank G. Decker and A. Lumpkin for their support and interest in this work. Thanks go to S. Kim, his magnet measurement crew, and L. Erwin for their help in preparing the measurement setup.

References

1. Y. Chung, "Compensation for the Eddy Current Effect in the APS Storage Ring Vacuum Chamber," LS Note 148, Argonne National Lab, 1990.
2. Y. Chung, J. Bridges, L. Emery and G. Decker, "Open Loop Compensation for the Eddy Current Effect in the APS Storage Ring Vacuum Chamber," *Proceedings of IEEE Particle Accelerator Conference*, San Francisco, 1991.
3 Y. Chung and K. Kim, unpublished.
4 Fermilab Electron Cooling Experiment, Design Report, FNAL (1978).
5. Y. Chung and J. Galayda, "Effect of Eddy Current in the Laminations on the Magnet Field," LS Note 200, ANL, 1992.
6. Y. Chung, L. Emery, and K. Kirchman, "Digital Signal Processing for Beam Position Feedback," LS Note 202, ANL, 1992.
7. A. Peled and B. Liu, *Digital Signal Processing*, John Wiley & Sons, 1976.
8. L. Turner, private communication.

9. W. Press et al., *Numerical Recipes in C*, Cambridge University Press, p. 528, 1989.
10. L. Emery, private communication.
11. W. Press et al., *Numerical Recipes in C*, Cambridge University Press, p. 60, 1989.